

Molecular Solubility and Hansen Solubility Parameters for the Analysis of Phase Separation in Bulk Heterojunctions

Duc T. Duong,¹ Bright Walker,² Jason Lin,¹ Chunki Kim,¹ John Love,¹
Balaji Purushothaman,³ John E. Anthony,³ Thuc-Quyen Nguyen¹

¹Center for Polymers and Organic Solids, Department of Chemistry and Biochemistry, University of California at Santa Barbara, Santa Barbara, California 93106

²Interdisciplinary School of Green Energy, Ulsan National Institute of Science and Technology, UNIST-gil 50, Ulsan 689-798, Republic of Korea

³Department of Chemistry, University of Kentucky, Lexington, Kentucky 40506-0055

Correspondence to: T.-Q. Nguyen (E-mail: quyen@chem.ucsb.edu)

Received 31 May 2012; revised 26 July 2012; accepted 6 August 2012; published online 24 August 2012

DOI: 10.1002/polb.23153

ABSTRACT: Although the fabrication procedures for bulk heterojunction (BHJ) solar cells are routinely optimized to accommodate new organic materials, the influence of solvent properties and cohesive forces on the film-forming process and the self-assembly of donor and acceptor molecules on the nanoscale are poorly understood. In this study, we measure the solubility of a variety of organic semiconductors in a range of solvents and calculate cohesive forces including dispersion forces, dipole interactions, and hydrogen bonding via Hansen Solubility Parameters (HSPs). HSPs were calculated by measuring the solubilities of various organic semiconductors in 27 solvents and the influence of solvent identity on film morphology of different BHJ mixtures was explored via atomic force microscopy (AFM). The possibility of correlations between HSPs and film

morphology was considered; however, it is apparent that the HSP values alone do not play a critical role in determining the morphology of the films of conjugated polymers and molecules. This collection of solubility data constitutes the first of its type for organic semiconducting materials, and may act as a useful reference for the organic semiconductor community to aid in the understanding and selection of solvents for donor-acceptor BHJ mixtures. © 2012 Wiley Periodicals, Inc. *J Polym Sci Part B: Polym Phys* 50: 1405–1413, 2012

KEYWORDS: atomic force microscopy AFM; bulk heterojunction; cohesive energy density; conjugated polymers; solubility; morphology

INTRODUCTION The discovery of efficient photo-induced charge transfer from semiconducting polymers to fullerene molecules in the 1990s^{1–3} positioned devices with the bulk heterojunction (BHJ) architecture among the most efficient organic solar cells known to date.^{4–8} The best reported single-junction organic photovoltaic devices operate only at 7–8% efficiency,⁹ whereas silicon-based devices achieve 15% (amorphous Si) to 20% (crystalline Si) efficiency.^{10,11} One of the biggest problems associated with OPVs' low efficiencies stems from an inadequate understanding of the intermolecular interactions between the organic species and their solvents and the resulting effects on film morphologies. Because numerous studies demonstrate that the nanostructures of organic thin films can have a major impact on the short-circuit current (I_{sc}) and the open circuit voltage (V_{oc}) of operating device,^{12–14} understanding the self-assembly process during BHJ formation would aid in the design of BHJ systems and potentially lead to higher power conversion efficiencies (PCEs).

In an ideal, conceptual BHJ device the organic donor and acceptor materials are solution-deposited from a common solvent to form thin films with interpenetrating networks of donor and acceptor materials on the order of 10–20 nm.^{15–17} This configuration allows for both efficient exciton dissociation at donor–acceptor (D–A) interfaces, and charge collection at the electrodes.^{18,19} However, the existence of charge recombination and trapping pathways can significantly hinder the overall PCE of BHJ devices.^{20–22} The formation of such traps is often attributed to the way in which donors, acceptors, and solvents interact during the spin casting and drying processes.²³ In the final film the two organic materials can mix to varying degrees and form domains with a wide range of sizes and shapes that may or may not be favorable for solar cell applications. Although it has been shown that fullerenes are able to quickly diffuse through conjugated polymers,²⁴ and that donor and acceptor materials are miscible in each other to a significant extent,²⁵ it is well known that the film history, especially processing solvents and solvent

Additional Supporting Information may be found in the online version of this article.

© 2012 Wiley Periodicals, Inc.

additives used to prepare the BHJ films, have a profound effect on their optoelectronic properties. A better understanding of the correlation between intermolecular forces and material distribution within BHJ films may help to accelerate the processing and fabrication of new D-A systems.

Because solubility is a key factor in the growth of organic crystals, we explored the solubility of various organic photovoltaic materials, the effect of solubility on the nanoscale morphology of various D-A mixtures, and its relationship to the intrinsic chemical properties of the molecular compounds. A basis for our initial studies begins with the concepts introduced by Hildebrand and Scott in 1950,^{26,27} who assigned solvents and organic molecules a value allowing prediction of their solubility. The Hildebrand solubility parameter (δ), defined by eq 1, predicts that solvents and organic compounds with similar cohesive energy density (E/V) would be more miscible.

$$\delta = (E/V)^{1/2} \quad (1)$$

However, this definition of solubility parameter is incomplete due to the fact that there is more than one mode of interaction between chemical compounds. These include van der Waals forces, dipole–dipole interactions, hydrogen bonding, electrostatic, induced dipole, and geometric considerations. In 1967, Charles Hansen proposed that each type of interaction can be given an individual parameter and formulated three solubility parameters for evaluating polymers.²⁸ The three Hansen Solubility Parameters (HSPs) correspond to the three most dominant forces governing organic polymers: London dispersion, dipole–dipole, and hydrogen bonding. These interactions thus correlate to the dispersive solubility parameter (δ_D), the polar solubility parameter (δ_P), and the H-bonding solubility parameter (δ_H), respectively. The relationship between the HSPs and the cohesive energy density is described by eq 2.

$$\delta^2 = (E/V) = \delta_D^2 + \delta_P^2 + \delta_H^2 \quad (2)$$

It is easy to imagine then that each organic molecule can be represented by a coordinate in 3-dimensional space, called Hansen space, in which the three Cartesian units are replaced with three HSPs. Therefore, the distance that separates two molecules in Hansen space should be inversely proportional to their miscibility (i.e., molecules that are miscible should be close to one another in Hansen space). This distance is termed the radius of interaction, R_A . The extent to which two materials will mix can be estimated by the relative energy difference (RED), as defined by eq 3, where R_0 is the radius of solubility, or the radius of the sphere in which good solvents are found. Two materials with a RED close to zero are expected to mix well or dissolve each other; a RED close to 1 implies intermediate miscibility while larger RED values indicate that the two materials should not mix well.

$$\text{RED} = R_A/R_0 \quad (3)$$

This method has been widely used to understand and predict the solubility and miscibility of organic materials in

many industries and research areas, leading to a large collection of reported HSPs for solvents and polymers.^{28–31} Recently, Hansen theory has been applied to a handful organic semiconducting materials.^{32,33} Our group has also applied HSP theory to identify several good solvents for preparing BHJs using 3,6-bis(5-(benzofuran-2-yl)thiophen-2-yl)-2,5-bis(2-ethylhexyl)pyrrolo[3,4-c]pyrrole-1,4-dione, **DPP(TBFu)₂**, and [6,6]-phenyl-C71-butyric acid methyl ester (**PC₇₁BM**).³⁴

In this study, we determined the solubility and HSPs for a variety of conjugated polymers and small molecules (Figure 1) commonly used in organic electronics, including polymeric donor materials such as poly(2-methoxy-5-(3',7'-dimethyl-octyloxy))-*p*-phenylene vinylene (**MDMO-PPV**), poly[2-methoxy-5-(2'-ethylhexyloxy)-*p*-phenylene vinylene] (**MEH-PPV**), and poly(3-hexylthiophene) (**P3HT**); light-emitting polymer poly(9,9-diethylfluorenyl-2,7-diyl) (**PFO**); small molecule donor materials **DPP(TBFu)₂** and 2,5-dihexyl-3,6-bis[4-(5-hexyl-2,2'-bithiophene-5-yl)phenyl]pyrrolo[3,4-c]pyrrole-1,4-dione (**DPP(PhTT)₂**); and acceptor compounds [6,6]-phenyl-C61-butyric acid methyl ester (**PC₆₁BM**), **PC₇₁BM** and 1,2,3,4,8,9,10,11 octafluoro 6,13-bis(*n*-octyldiisopropylsilyl)pentacene (**F8NODIPS**). The solubilities of these materials in a wide range of solvents are valuable for designing device structures, especially in multilayer systems that require the use of orthogonal solvents. In addition to the generation of a comprehensive collection of data on the solubility of some common organic semiconductors in this work, we also use atomic force microscopy (AFM) to examine correlations between the solubility characteristics of different combinations of materials and solvents with their characteristic film surface morphologies.

RESULTS AND DISCUSSION

Solubilities and Hansen Solubility Parameters of Organic Semiconductors

The solubilities of all organic compounds in 27 different solvents were determined by one of two methods. For small molecules, saturated solutions were made, filtered, diluted by factors ranging from 100 to 10,000 and analyzed using UV-visible spectroscopy. In the case of polymers, only estimates of their solubilities can be acquired due to the tendency of concentrated solutions to gelate and form highly viscous solutions. Solubilities for polymers were evaluated by mixing a weighed amount of polymer with solvent, heating at 60 °C with magnetic stirring overnight and allowing to return to room temperature. Solvents which yielded qualitatively homogeneous solutions were considered to be “good.” Different concentrations of polymer were evaluated by adding additional polymer to the test solvent and repeating the procedure for concentrations of 1, 2, 4, 6, 8, and 10 mg/mL. The maximum measured solubility for polymers was chosen to be 10 mg/mL since higher concentrations are often very viscous and difficult to categorize as being solutions, dispersions, or gels. Raw absorption spectra, calibration curves, and more detailed procedures can be found in Supporting Information Figures S1–S3. Table 1 summarizes the solubility results.

The HSPs for each molecule were determined using software developed by Abbott and Hansen wherein good solvents are

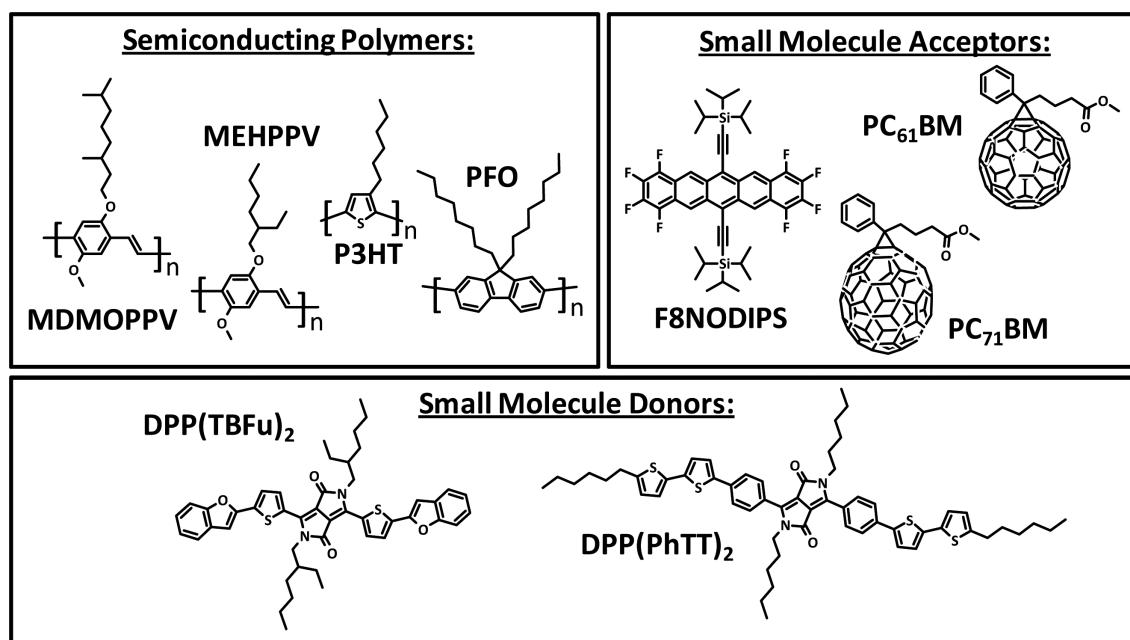


FIGURE 1 Chemical structures of organic semiconducting materials used in this work.

assigned a value of “1” and bad solvents a value of “0.” For each test material, the software creates a sphere in Hansen space containing the coordinates of good solvents while excluding the coordinates of bad solvents, where the center of the sphere represents the Hansen parameters of the test material and the radius of the sphere is R_0 . The definition of “good” solvent may have some variability since a solvent that is able to dissolve 1, 10, or 100 mg/mL is considered “good” depending on the context. Several cutoff values which yielded good fits were chosen for each small molecule and the generated HSPs were averaged. For polymers, solvents were considered “good” if they were able to form homogeneous solutions. Cut-off concentrations of 1 mg/mL and at 10 mg/mL were used to calculate polymer HSPs. Errors shown represent the standard deviations of the mean for HSP values using different cutoff values and are not reported for polymers since only two cutoff values were used. R_0 values were taken at the 10 mg/mL solubility level with the exception of **DPP(TBFu)₂**, for which the 10 mg/mL level does not yield a good fit and a previously reported value at the 3 mg/mL solubility level was used. For comparison, RED values for each material with **PC₆₁BM** are calculated. Table 2 summarizes all of the obtained solubility parameters. As expected, the measured parameters for the two fullerenes (**PC₆₁BM** and **PC₇₁BM**) and the two poly(phenylene vinylene) (**MDMO-PPV** and **MEH-PPV**) are very similar within experimental error.

Optical Properties of Films Prepared from Different Solvents

Out of all the organic molecules under consideration, we chose to make three series of films comprising of **MDMO-PPV**, **MEH-PPV**, and **P3HT** as donor materials and **PC₆₁BM** as the acceptor in different solvents. Films were prepared by

spin-casting from solutions of 20:80 **MDMO-PPV:PC₆₁BM**, 20:80 **MEH-PPV:PC₆₁BM** and 50:50 **P3HT:PC₆₁BM** at total concentrations of 15 mg/mL (PPVs) and 20 mg/mL (P3HT) onto indium tin-oxide (ITO) coated glass substrates with a ~50 nm layer of poly(3,4-ethylenedioxothiophene):poly(styrene sulfonate), PEDOT:PSS. The particular ratios and concentrations were chosen based on fabrication parameters that typically yield efficient devices.^{35–41} Raw absorptions of blended films for all three systems are summarized in the Supporting Information Figure S4. Absorption maxima at 330 nm are assigned to **PC₆₁BM** and those in the visible range are attributed to the polymeric donors. The spectral data suggest that annealing has no significant effect on the structural order of **MDMO-PPV:PC₆₁BM** and **MEH-PPV:PC₆₁BM** thin films with the exception of films cast from CS₂. In this case a dramatic increase in the absorption intensity ratio between polymeric bands and **PC₆₁BM** band is attributed to phase aggregation of **PC₆₁BM** molecules. Conversely, an increase in overall absorption of **P3HT:PC₆₁BM** thin films following annealing is consistent with previous reports and has been ascribed to an increase in crystallinity of the donor and acceptor domains leading to more efficient absorption via $\pi-\pi^*$ transitions.^{36,42–44} All alterations in the absorption bands for these BHJ thin films are consistent with morphological changes observed microscopically.

Analysis of Film Morphologies and Feature Size

In order to investigate relationships between solubility parameters and film surface structure, morphologies of blended films were analyzed using tapping-mode AFM. Although AFM measurements do not provide explicit information about the 3-dimensional structure of films, or the distribution of materials beneath the surface, the surface structure of BHJ films as measured by AFM often shows

TABLE 1 Solubility of Organic Semiconducting Materials in Organic Solvents

Solvents	PC ₆₁ BM (mg/mL)	PC ₇₁ BM (mg/mL)	DPP(TBFu) ₂ (mg/mL)	F8-NODIPS (mg/mL)	DPP(PhTT) ₂ (mg/mL)	MDMO-PPV (mg/mL)	MEH-PPV (mg/mL)	P3HT (mg/mL)	PFO (mg/mL)
<i>o</i> -Dichlorobenzene	107	203	4.5	>120	0.9	>10	>10	>10	<1
Chlorobenzene	37.1	60.6	3.4	>120	<0.3	>10	>10	>10	6–10
CS ₂	207	142	4.5	>120	1.6	>10	>10	>10	>10
CHCl ₃	27	61.1	15.3	36.3	11.3	>10	>10	>10	>10
THF	1.5	3.5	4.4	>120	0.4	>10	>10	1–2	6–10
Pyridine	12.3	25.2	0.8	19.4	<0.3	>10	>10	<1	<1
<i>o</i> -Xylene	20.5	66.2	1.5	>120	<0.3	>10	>10	1–2	2–4
Trichloroethylene	41.8	159.9	7.2	36.5	1.1	>10	>10	>10	>10
Thiophene	6.1	19.3	7.2	110	1.0	>10	>10	4–6	6–10
1,2-Dichloroethane	2.7	3.5	0.6	25.7	<0.3	>10	>10	<1	<1
Toluene	10.9	27.4	1.3	119	<0.3	>10	>10	1–2	6–10
Dioxane	1.3	1.0	0.6	>120	<0.3	4–6	>10	<1	<1
Nitrobenzene	15.6	25.7	1.0	>120	<0.3	6–10	>10	<1	<1
DMF	2.1	<0.5	<0.5	<0.3	<0.3	<1	<1	<1	<1
Triethylamine	0.5	<0.5	<0.5	50.4	<0.3	<1	<1	<1	<1
Ethyl acetate	<0.3	<0.5	<0.5	13.2	<0.3	<1	<1	<1	<1
DMSO	<0.3	<0.5	<0.5	<0.3	<0.3	<1	<1	<1	<1
Hexane	<0.3	<0.5	<0.5	67.4	<0.3	<1	<1	<1	<1
Isopropanol	<0.3	<0.5	<0.5	0.4	<0.3	<1	<1	<1	<1
Acetone	<0.3	<0.5	<0.5	1.0	<0.3	<1	<1	<1	<1
2-Methyl-2-butanol	<0.3	<0.5	<0.5	9.4	<0.3	<1	<1	<1	<1
Acetonitrile	<0.3	<0.5	<0.5	<0.3	<0.3	<1	<1	<1	<1
Octane	<0.3	–	–	65.1	<0.3	<1	<1	<1	<1
1-Methylpyrrole	31.5	26.8	0.6	1.62	<0.3	>10	>10	<1	<1
<i>n</i> -Tributyl phosphate	0.5	2.4	<0.5	6.6	<0.3	<1	<1	<1	<1
1,1,2,2-tetrabromooethane	128	>480	8.3	0.7	0.6	4–6	4–6	<1	<1
Diiodomethane	50.0	356.8	<0.5	<0.3	<0.3	<1	<1	<1	<1

correlation to device characteristics and provides information about the surface distribution of materials in BHJs.^{16,45–49} For instance, conducting AFM studies have shown that topographic features often correspond to regions of predominantly p or n type conductivity and thus, a correlation to the distribution of p-type and n-type materials parallel to the substrate.⁵⁰

Figure 2 depicts topographic images of as-cast and annealed 20:80 MDMO-PPV:PC₆₁BM films. Particle-like domains with sizes in the range of 100–500 nm are observed for as-cast films in all selected solvents except for CS₂, which shows a less cluster-like morphology. Sariciftci and coworkers previously verified that these “nanoclusters” are composed of a fullerene center embedded within a polymer-rich outer layer.⁵¹ The AFM images here demonstrate that cluster sizes are strongly dependent on the spin-casting solvent and how well it can solubilize PC₆₁BM. The solubilities of PC₆₁BM in pyridine and toluene, 12.3 mg/mL and 10.9 mg/mL respectively, are the lowest out of the seven chosen solvents. As a result, MDMO-PPV:PC₆₁BM films deposited from these two solvents exhibit the largest nanocluster domains. Nanocluster

sizes were measured using several techniques including power spectral density (PSD), grain size calculations, 2D Fourier transform, and manual cross-section analysis. A summary of the average particle size for both as-cast and annealed films is shown in Table 3. It is important to note that the values reported for films spin-cast from CS₂ [Figure 2(b, i)] denote feature sizes rather than particle sizes.

Thermal annealing of these films at 140 °C, which is well above the glass transition temperatures (T_g) of the all three semiconducting polymers and PC₆₁BM,^{52–54} allowed the particles to fuse into larger domains. The degree to which this process occurs is controlled by the concentration of clusters in the films, the interparticle distance and the molecular packing within the polymer-rich outer layer. As-cast films deposited from chloroform and trichloroethylene, for instance, are comprised of similar cluster sizes and interparticle distances. However, the annealed film for chloroform boasts larger clusters (288 ± 77 nm) than that for trichloroethylene (235 ± 84 nm). Similarly, films deposited from toluene and pyridine show similar cluster sizes but very different interparticle distances (on average 50–200 nm for toluene

TABLE 2 Summarized Hansen Solubility Parameters for Various Organic Semiconductors

	δ_D (MPa $^{1/2}$)	δ_P (MPa $^{1/2}$)	δ_H (MPa $^{1/2}$)	R_0	RED (PC ₆₁ BM)
Small molecules					
PC ₆₁ BM	19.89 ± 0.34	5.68 ± 1.03	3.64 ± 0.92	6.6	0.00
PC ₇₁ BM	20.16 ± 0.28	5.37 ± 0.80	4.49 ± 0.57	7.0	0.15
DPP(TBFu) ₂	19.33 ± 0.05	4.78 ± 0.50	6.26 ± 0.48	5.1	0.59
F8-NODIPS	18.48 ± 0.28	2.62 ± 0.56	3.24 ± 0.91	8.1	0.52
DPP(PhTT) ₂	19.64 ± 0.32	3.54 ± 0.56	6.12 ± 0.65	—	—
Polymers					
MDMO-PPV	19.06	5.62	5.28	5.5	0.42
MEH-PPV	19.06	5.38	5.44	6.0	0.41
P3HT	18.56	2.88	3.19	3.6	1.08
PFO	18.55	2.8	4.51	4.1	0.98

and < 50 nm for pyridine). In stark contrast to the fused nanoclusters, porous networks of **MDMO-PPV** polymers (average pore size in these films is calculated to be 190 ± 32 nm) and micron-sized aggregates are observed in the annealed films deposited from CS₂. This is consistent with the film optical data and suggests that the PC₆₁BM domains in the underlying film are quite mobile and can quickly diffuse out of the internal structure to form larger aggregates. The diffusion of PC₆₁BM is consistent with reports on the

diffusion of PC₆₁BM through other conjugated polymers; however, our data suggest that the diffusivity of PC₆₁BM may be affected by the solvent used to process the film.²⁴ Longer annealing time would lead to larger aggregates.⁴⁵

The morphologies of **MEH-PPV:PC₆₁BM** (Supporting Information Fig. S5) are in striking contrast to those of **MDMO-PPV**, even though there is little structural difference between the two polymers (3,7 dimethyloctyl vs. 2-ethylhexyl solubilizing groups), HSP values or the optical properties of the films.

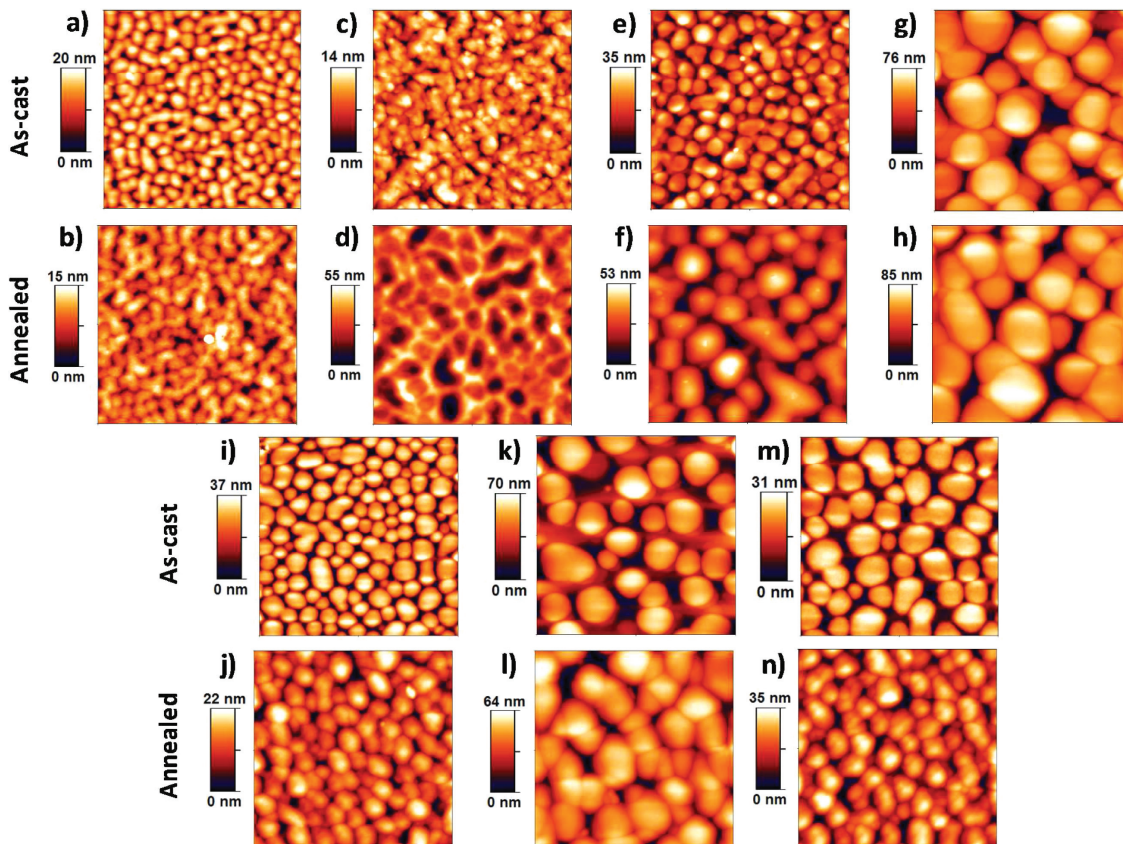


FIGURE 2 AFM topography images (2 $\mu\text{m} \times 2 \mu\text{m}$) of as-cast and annealed films of **MDMO-PPV:PC₆₁BM** spin-casted from chlorobenzene (a, b), CS₂ (c, d), CHCl₃ (e, f), pyridine (g, h), trichloroethylene (i, j), toluene (k, l), and 1-methylpyrrole (m, n).

TABLE 3 Average Particle Sizes in 20:80 MDMO-PPV:PC₆₁BM Films Spin-Casted From Different Solvents

Solvents	As-Cast MDMO-PPV: PC ₆₁ BM Particle size (nm)		PC ₆₁ BM Particle size (nm)
	PC ₆₁ BM Particle size (nm)	PC ₆₁ BM Particle size (nm)	
Chlorobenzene	148 ± 32	152 ± 33	
CS ₂	100	176	
CHCl ₃	184 ± 43	288 ± 77	
Pyridine	430 ± 90	441 ± 93	
Trichloroethylene	189 ± 30	235 ± 84	
Toluene	391 ± 53	410 ± 74	
1-Methylpyrrole	274 ± 60	256 ± 36	

The characteristic bubble-like features observed in **MDMO-PPV:PC₆₁BM** are not seen for **MEH-PPV:PC₆₁BM** films cast from any of the solvents explored, either before or after annealing. It is possible that because there is a larger volume of open space in between the alkyl chains in **MDMO-PPV**, intercalation of **PC₆₁BM** between the chains can occur more readily, affecting the ability of the fullerene to diffuse through the film and the fundamental composition of the solid.

In contrast to the poly(phenylene vinylene) polymers, AFM images of 50:50 **P3HT:PC₆₁BM** films (Figure 3) do not show large clusters or domains and all exhibit roughness RMS of less than 1 nm with an exception of the annealed film from CS₂ (~2 nm). In addition, pores with an average diameter of 67 ± 17 nm and depth of 5–10 nm in both as-cast and annealed films spin-casted from CS₂ are observed. Phase images corresponding to the height images of **P3HT:PC₆₁BM** films are reported and discussed in the Supporting Information Figure S6. It is noteworthy that feature sizes in 50:50 **P3HT:PC₆₁BM** films are small and do not dramatically vary between the five solvents. This may be explained by similar solubilizing properties of the five solvents for both donor and acceptor materials.

Next, we keep the solvent constant (CHCl₃) and compare films of solid materials with different HSPs admixed with **PC₆₁BM**. AFM images of **MDMO-PPV:PC₆₁BM**, **MEH-PPV:PC₆₁BM**,

P3HT:PC₆₁BM, **PFO:PC₆₁BM**, **DPP(TBFu)₂:PC₆₁BM**, and **DPP(PhTT)₂:PC₆₁BM** films are reported in Figure 4. Although HSPs quantify the cohesion energies of equilibrated solutes in solution and spin-coated BHJ mixtures are better described as non-equilibrium, solid-state mixtures, we nonetheless sought to identify correlations between the HSPs of different donor materials and their morphological behavior in BHJs with **PC₆₁BM**. If there were a correlation between cohesion energies of materials in solution and in the solid state, we might consider **PC₆₁BM** to be a kind of solid solvent, and the BHJ film to be a solid solution. In this case one might expect materials having smaller REDs with **PC₆₁BM** to be more likely to form homogenous, solid solutions and form smoother films. However, this is not the case.

In general, materials with larger R_0 values (materials which are soluble in a wider range of solvents) are predicted to mix better with other solvents, but these are not the trends we observe in the solid state. Out of the small molecules, there appears to be a trend where the feature size and film roughness are larger for the materials with larger R_0 values, the opposite of the expected trend. **DPP(PhTT)₂** is soluble in the smallest range of solvents and shows the smallest phase separation while **DPP(TBFu)₂** has intermediate solubility and shows intermediate domains. The roughest films and most drastic phase separation occur in **MDMO-PPV** and **PFO**, two polymers which have large free volumes between alkyl chains, allowing **PC₆₁BM** to diffuse more readily through the structure, enabling the formation of larger aggregates.

As one might expect, spin-casting is a complex process wherein additional factors such as solvent evaporation rate, film thickness, and type of substrate can affect the crystallization kinetics and thereby the final morphology of the film.^{55–57} To investigate the effect of evaporation rate and film drying kinetics on morphology, we prepared **MDMO-PPV:PC₆₁BM** films at a variety of spin-rates (600 rpm–4500 rpm) and by drop-casting. AFM images of the films are shown in Figure 5. Because films spin-cast at higher spin rates evaporate more quickly, this allows us to observe a qualitative relationship between solvent evaporation rate and surface morphology. While all of the films exhibit similar

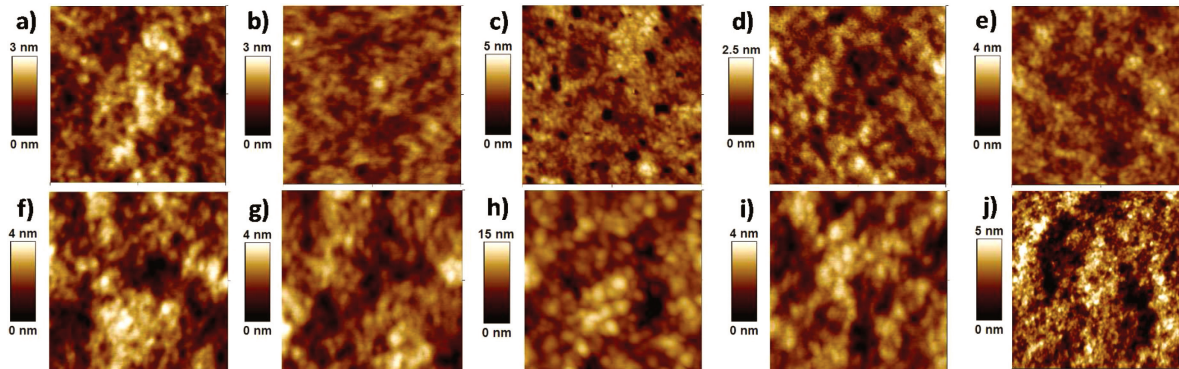


FIGURE 3 AFM topography images (500 nm × 500 nm) of as-cast (top) and annealed films (bottom) of **P3HT:PC₆₁BM** spin-casted from *o*-dichlorobenzene (a, f), chlorobenzene (b, g), CS₂ (c, h), CHCl₃ (d, i), and trichloroethylene (e, j). (Image "j" is a 2 μm × 2 μm scan).

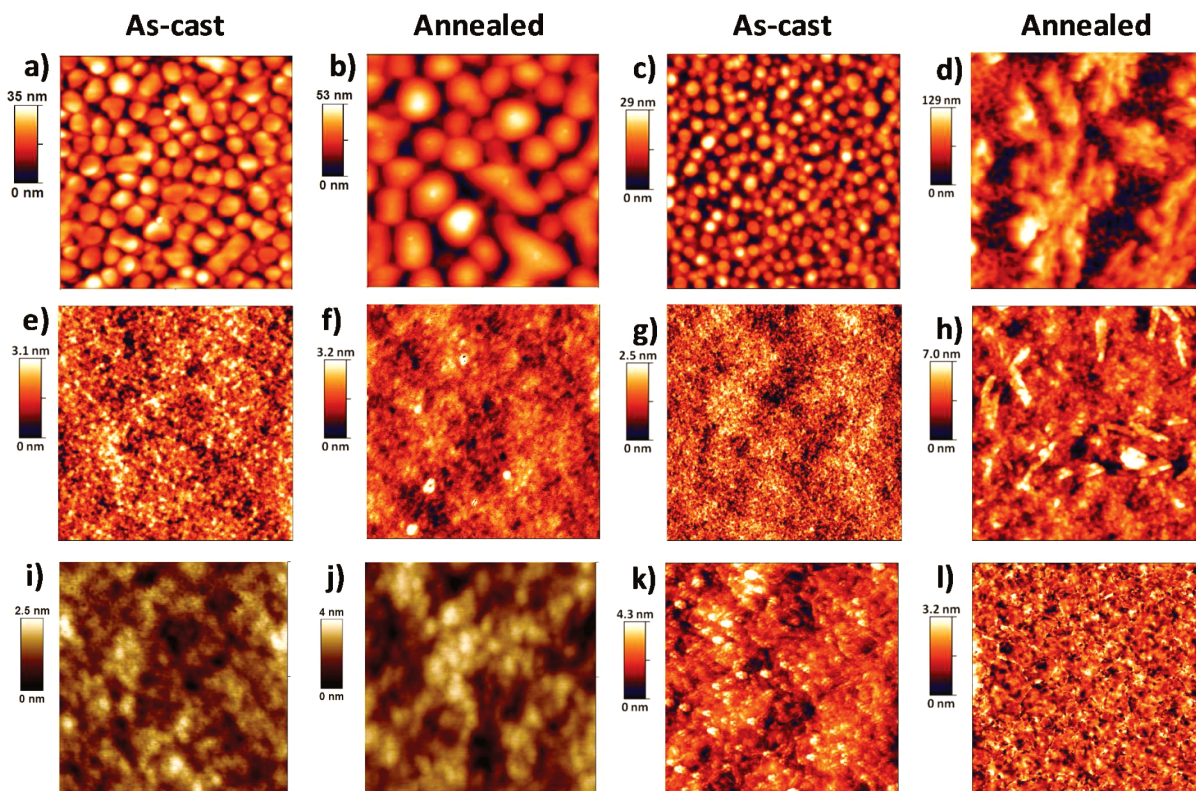


FIGURE 4 AFM topographic images ($2 \mu\text{m} \times 2 \mu\text{m}$) of as-cast (a, c, e, g, i, k) and annealed (b, d, f, h, j, l) films of **MDMO-PPV:PC₆₁BM** (a, b), **PFO:PC₆₁BM** (c, d), **MEH-PPV:PC₆₁BM** (e, f), **DPP(TBFu)₂:PC₇₁BM** (g, h), **P3HT:PC₆₁BM** (i, j), and **DPP(PhTT)₂:PC₇₁BM** (k, l). All films were spin-cast from CHCl₃; polymer blends were annealed at 140 °C for 10 min while small molecules were annealed at 100 °C for 10 min.

bubble-like features, a clear trend is observed where the domain size of the features (Table 4) becomes larger for slower spin-rates. The largest features are observed in the drop-cast film (1500 nm in diameter), in which the solvent evaporates the most slowly. Thus, it is clear that the kinetic

processes that occur during film drying have a strong effect on domain size in the **MDMO-PPV:PC₆₁BM** system. It appears that slower evaporation rates allow more time for the materials to self-assemble into thermodynamically stable arrangement, leading to larger domain sizes.

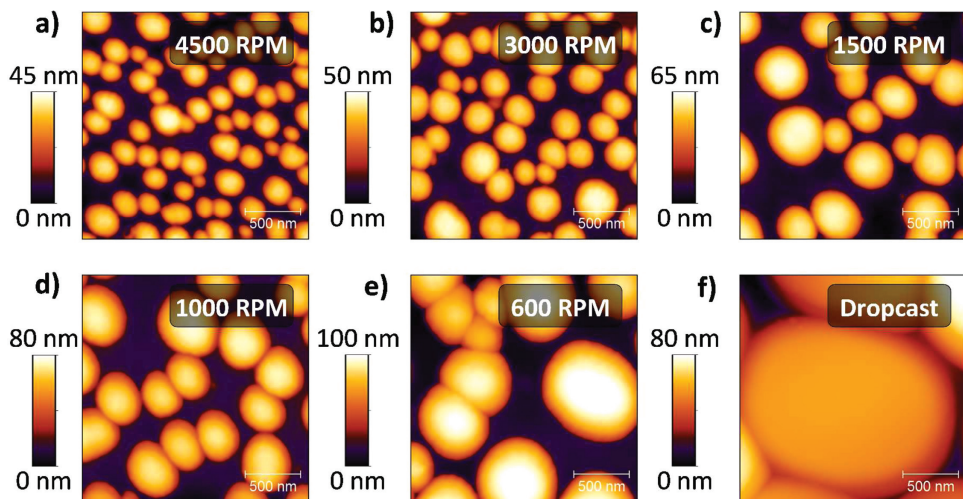


FIGURE 5 AFM topography images ($2 \mu\text{m} \times 2 \mu\text{m}$) of **MDMO-PPV:PC₆₁BM** spin-cast from chlorobenzene at (a) 4500 rpm, (b) 3000 rpm, (c) 1500 rpm, (d) 1000 rpm, and (e) 600 rpm. The surface topography of an **MDMO-PPV:PC₆₁BM** film drop-cast from chlorobenzene is shown in (f).

TABLE 4 Estimated Domain Sizes in As-Cast 20:80 **MDMO-PPV:PC₆₁BM** Films Spin-Casted From Chlorobenzene at Different Spin Rates

Spin Rate (rpm)	Domain Size (nm)
0	1,500
600	450
1000	340
1500	310
3000	220
4500	190

Although we cannot yet provide a quantitative relationship between the BHJ morphology, cohesive energy density, and drying rates, the solubility data and extracted HSPs are crucial in deconvoluting the film forming process. For instance, Li et al. showed that increasing the solubility of **C₆₀** can lead to higher **P3HT** crystallinity in **P3HT:C₆₀** thin films.⁵⁸ They observed that the formation of **C₆₀** crystallites hinders the subsequent crystallization of **P3HT** from solution and that the use of additives that are good solvents for **C₆₀** can improve film formation. On the contrary, Yao et al. saw that cluster formation of **PCBM** can improve the crystallization of **P3HT** in blended films.⁵⁹ Clearly, the solubility of individual components plays an important role in determining which component will begin to crystallize first. In several case studies, the formation of nanocrystalline structures in BHJ thin films is explained in terms of a phase diagram for the polymer-fullerene-solvent mixture as well as the Flory-Huggins interaction parameter, both of which can be calculated from solubilities and solubility parameters.^{53,60,61} Though solubility alone cannot explain the intricate process BHJ formation, it is an essential component in understanding and controlling the process of BHJ formation.

CONCLUSIONS

In conclusion, we have measured the solubility of various organic semiconductors in 27 different solvents. From this data, the corresponding HSPs were calculated for each material. While HSPs are intimately related to the miscibility of different materials, we conclude that differences in cohesion energies play a secondary role to kinetic factors such as solvent evaporation rate, crystallization rates, and the diffusion of materials in determining film morphology. We anticipate that in combination with diffusion and kinetic studies of film formation, Hansen's theory may prove to be a powerful tool in predicting the morphology evolution in BHJ systems during solvent processing and help lead to more intelligent designs of new BHJ materials as well as a better solvent selection process.

EXPERIMENTAL

All polymers, fullerenes, and solvents were purchased and used without further purifications. **DPP(TBFu)₂**, **DPP(PhTT)₂**, and **F8NODIPS** were synthesized according to references Refs. 62–64, respectively.

Thin films were prepared by first spin-casting PEDOT:PSS (H.C. Stark Baytron P 4083) onto cleaned glass substrates at 2500 rpm for 60 s followed by thermal annealing at 140 °C for 30–40 min. All BHJ layers were spin-cast at 1500 rpm for 60 s from solutions of 20:80 **MDMO-PPV:PC₆₁BM**, 20:80 **MEH-PPV:PC₆₁BM**, and 50:50 **P3HT:PC₆₁BM** at solid concentrations of 15 mg/mL, 15 mg/mL, and 20 mg/mL, respectively. Polymer solutions were allowed to stir magnetically at 60 °C for at least 12 h prior to use, while small molecule solutions were heated at 60 °C for at least 2 h prior to use. Polymer films were annealed at 140 °C for 30 min, while small molecule films were annealed at 100 °C for 10 min. UV-visible spectroscopy was performed on a Beckman Coulter DU800 Spectrophotometer. AFM images of **MDMO-PPV** and **MEH-PPV** films were collected in air under atmospheric conditions using the Innova scanning probe microscope (Bruker). **P3HT** films were collected in nitrogen atmosphere using a Multi-mode scanning probe microscope (Bruker). All imaging were done using silicon Vista probes with spring constants of 3 N m⁻¹ and resonant frequencies of 62 kHz.

ACKNOWLEDGMENTS

The authors gratefully acknowledge helpful discussions from Prof. Steven Abbott. The authors thank the NSF-SOLAR (Jason Lin and John Love), Office of Naval Research (C. Kim and B. Walker), and the Camille Dreyfus Teacher-Scholar Awards Program for the financial support. T.-Q. Nguyen is an Alfred P. Sloan Foundation Research Fellow.

REFERENCES AND NOTES

- 1 Sariciftci, N. S.; Smilowitz, L.; Heeger, A. J.; Wudl, F. *Science* **1992**, *258*, 1474–1476.
- 2 Kraabel, B.; Lee, C. H.; McBranch, D.; Moses, D.; Sariciftci, N. S.; Heeger, A. J. *Chem. Phys. Lett.* **1993**, *213*, 389–394.
- 3 Kraabel, B.; McBranch, D.; Sariciftci, N. S.; Moses, D.; Heeger, A. J. *Phys. Res. B* **1994**, *50*, 18543–18552.
- 4 Yu, G.; Gao, J.; Hummelen, J. C.; Wudl, F.; Heeger, A. J. *Science* **1995**, *270*, 1789–1791.
- 5 Gunes, S.; Neugebauer, H.; Sariciftci, N. S. *Chem. Rev.* **2007**, *107*, 1324–1338.
- 6 Coakley, K. M.; McGehee, M. D. *Chem. Mater.* **2004**, *16*, 4533–4542.
- 7 Scharber, M. C.; Mühlbacher, D.; Koppe, M.; Denk, P.; Waldau, C.; Heeger, A. J.; Brabec, C. J. *Adv. Mater.* **2006**, *18*, 789–794.
- 8 Roncali, J. *Acc. Chem. Res.* **2009**, *42*, 1719–1730.
- 9 Li, G.; Zhu, R.; Yang, Y. *Nat. Photon.* **2012**, *6*, 153–161.
- 10 Carlson, D. E.; Wronski, C. R. *Appl. Phys. Lett.* **1976**, *28*, 671–673.
- 11 Schultz, O.; Glunz, S. W.; Willeke, G. P. *Prog. Photovolt. Res. Appl.* **2004**, *12*, 553–558.
- 12 Geens, W.; Martens, T.; Poortmans, J.; Aernouts, T.; Manca, J.; Lutsen, L.; Heremans, P.; Borghs, S.; Mertens, R.; Vandervanderzande, D. *Thin Solid Films* **2004**, *451–452*, 498–502.
- 13 You, H.-L.; Zhang, C.-F. *Chin. Phys. B* **2009**, *18*, 349–356.
- 14 Yamanari, T.; Taima, T.; Sakai, J.; Saito, K. *Sol. Energ. Mater. Sol. C* **2009**, *93*, 759–761.

- 15** Muller, C.; Ferenczi, T. A. M.; Campoy-Quiles, M.; Frost, J. M.; Bradley, D. D. C.; Smith, P.; Stingelin-Stutzmann, N.; Nelson, J. *Adv. Mater.* **2008**, *20*, 3510–3515.
- 16** Dante, M.; Peet, J.; Nguyen, T.-Q. *J. Phys. Chem. C* **2008**, *112*, 7241–7249.
- 17** Moon, J. S.; Lee, J. K.; Cho, S.; Byun, J.; Heeger, A. J. *Nano Lett.* **2009**, *9*, 230–234.
- 18** Bredas, J.-L.; Norton, J. E.; Cornil, J.; Coropceanu, V. *Acc. Chem. Res.* **2009**, *42*, 1691–1699.
- 19** Potscavage, W. J.; Sharma, A.; Kippelen, B. *Acc. Chem. Res.* **2009**, *42*, 1758–1767.
- 20** Chiguvare, Z.; Dyakonov, V. *Phys. Rev. B* **2004**, *70*, 235207.
- 21** Mandoc, M. M.; Veurman, W.; Koster, L. J. A.; Koetse, M. M.; Sweenissen, J.; de Boer, B.; Blom, P. W. M. *J. Appl. Phys.* **2007**, *101*, 104512.
- 22** Tong, M.; Coates, N. E.; Moses, D.; Heeger, A. J.; Beaupre, S.; Leclerc, M. *Phys. Rev. B* **2010**, *81*, 125210.
- 23** Dyakonov, V. *Appl. Phys. A Mater.* **2004**, *79*, 21–25.
- 24** Treat, N. D.; Brady, M. A.; Smith, G.; Toney, M. F.; Kramer, E. J.; Hawker, C. J.; Chabiny, M. L. *Adv. Energy Mater.* **2011**, *1*, 82–89.
- 25** Yin, W.; Dadmun, M. *ACS Nano* **2011**, *5*, 4756–4768.
- 26** Hildebrand, J.; Scott, R. L. *The Solubility of Nonelectrolytes*, 3rd ed.; Reinhold: New York, **1950**.
- 27** Hildebrand, J.; Scott, R. L. *Regular Solutions*; Prentice-Hall Inc.: Englewood Cliffs, **1962**.
- 28** Hansen, C. M. *Hansen Solubility Parameters: A User's Handbook*, 2nd ed.; CRC Press: Boca Raton, **2007**; Chapter 1.
- 29** Wohlfarth, C. In *CRC Handbook of Chemistry and Physics*, 90th ed. (Internet Version **2010**); Lide, D. R., Ed.; CRC Press/Taylor and Francis: Boca Raton, FL; pp 13–70.
- 30** Barton, A. F. M. *Chem. Rev.* **1975**, *75*, 731–753.
- 31** Barton, A. F. M. *CRC Handbook of Solubility Parameters and Other Cohesion Parameters*; CRC Press: Boca Raton, FL, **1983**; Chapter 6.
- 32** Machui, F.; Abbott, S.; Waller, D.; Koppe, M.; Brabec, C. *J. Macromol. Chem. Phys.* **2011**, *212*, 2159–2165.
- 33** Mahui, F.; Langner, S.; Zhu, X.; Abbott, S.; Brabec, C. *J. Sol. Energ. Mater. Sol. Cells* **2012**, *100*, 138–146.
- 34** Walker, B.; Tamayo, A. B.; Duong, D.; Dang, X.-D.; Kim, C.; Granstrom, J.; Nguyen, T.-Q. *Adv. Energy Mater.* **2011**, *1*, 221–229.
- 35** Shaheen, S. E.; Brabec, C. J.; Sariciftci, N. S.; Padinger, F.; Fromherz, T.; Hummelen, J. C. *Appl. Phys. Lett.* **2001**, *78*, 841–843.
- 36** Padinger, F.; Rittberger, R. S.; Sariciftci, N. S. *Adv. Funct. Mater.* **2003**, *13*, 85–88.
- 37** Zhang, F. L.; Johansson, M.; Andersson, M. R.; Hummelen, J. C.; Inganäs, O. *Synth. Met.* **2003**, *137*, 1401–1402.
- 38** Tuladhar, S. M.; Sims, M.; Choulis, S. A.; Nielsen, C. B.; George, W. N.; Steinke, J. H. G.; Bradley, D. D. C.; Nelson, J. *Org. Electron.* **2009**, *10*, 562–567.
- 39** Martens, T.; D'Haen, J.; Munters, T.; Beelen, Z.; Goris, L.; Manca, J.; D'Olieslaeger, M.; Vanderzande, D.; Schepper, L. D.; Andriessen, R. *Synth. Met.* **2003**, *138*, 243–247.
- 40** Baek, W.-H.; Yoon, T.-S.; Lee, H. H.; Kim, Y.-S. *Org. Electron.* **2010**, *11*, 933–937.
- 41** Kim, Y.; Choulis, S. A.; Nelson, J.; Bradley, D. D. C.; Cook, S.; Durrant, J. R. *J. Mater. Sci.* **2005**, *40*, 1371–1376.
- 42** Chirvase, D.; Parisi, J.; Hummelen, J. C.; Dyakonov, V. *Nanotechnology* **2004**, *15*, 1317–1323.
- 43** Erb, T.; Zhokhavets, U.; Gobsch, G.; Raleva, S.; Stühn, B.; Schiliinsky, P.; Waldauf, C.; Brabec, C. J. *Adv. Funct. Mater.* **2005**, *15*, 1193–1196.
- 44** Erb, T.; Zhokhavets, U.; Hoppe, H.; Gobsch, G.; Al-Ibrahim, M.; Ambacher, O. *Thin Solid Films* **2006**, *511*–*512*, 483–485.
- 45** Hoppe, H.; Niggemann, M.; Winder, C.; Kraut, J.; Hiesgen, R.; Hinsch, A.; Meissner, D.; Sariciftci, N. S. *Adv. Funct. Mater.* **2004**, *14*, 1005–1011.
- 46** Groves, C.; Reid, O. G.; Ginger, D. S. *Acc. Chem. Res.* **2010**, *43*, 612–620.
- 47** Hoven, C. V.; Dang, X.-D.; Coffin, R. C.; Peet, J.; Nguyen, T.-Q.; Bazan, G. C. *Adv. Mater.* **2010**, *22*, E63–E66.
- 48** Xin, H.; Kim, F. S.; Jenekhe, S. A. *J. Am. Chem. Soc.* **2008**, *130*, 5424–5425.
- 49** Nguyen, L. H.; Hoppe, H.; Erb, T.; Günes, S.; Gobsch, G.; Sariciftci, N. S. *Adv. Funct. Mater.* **2007**, *17*, 1071–1078.
- 50** Dang, X.; Tamayo, A.; Seo, J.; Hoven, C.; Walker, B.; Nguyen, T. *Adv. Funct. Mater.* **2010**, *20*, 3314–3321.
- 51** Hoppe, H.; Glatzel, T.; Niggemann, M.; Schwinger, W.; Schaeffler, F.; Hinsch, A.; Lux-Steiner, M. Ch.; Sariciftci, N. S. *Thin Solid Films* **2006**, *511*–*512*, 587–592.
- 52** Conings, B.; Bertho, S.; Vandewal, K.; Senes, A.; D'Haen, J.; Manca, J.; Janssen, R. A. *J. Appl. Phys. Lett.* **2010**, *96*, 163301.
- 53** Zhao, J.; Swinnen, A.; Van Assche, G.; Manca, J.; Vanderzande, D.; Van Mele, B. *J. Phys. Chem. B* **2009**, *113*, 1587–1591.
- 54** Liu, J.; Guo, T.-F.; Yang, Y. *J. Appl. Phys.* **2002**, *91*, 1595–1600.
- 55** Wang, T.; Dunbar, A. D. F.; Staniec, P. A.; Pearson, A. J.; Hopkinson, P. E.; MacDonald, J. E.; Lilliu, S.; Pizsey, C.; Terrill, N. J.; Donald, A. M.; Ryan, A. J.; Jones, R. A. L.; Lidzey, D. G. *Soft Matter* **2010**, *6*, 4128–4134.
- 56** Van Bavel, S.; Sourty, E.; De With, G.; Frolic, K.; Loos, J. *Macromolecules* **2009**, *42*, 7396–7403.
- 57** He, C.; Germack, D. S.; Kline, R. J.; Delongchamp, D. M.; Fischer, D. A.; Snyder, C. R.; Toney, M. F.; Kushmerick, J. G.; Richter, L. *J. Sol. Energ. Mater. Sol. C* **2011**, *95*, 1375–1381.
- 58** Li, L.; Tang, H.; Wu, H.; Lu, G.; Yang, X. *Org. Electron.* **2009**, *10*, 1334–1344.
- 59** Yao, Y.; Hou, J.; Xu, Z.; Li, G.; Yang, Y. *Adv. Funct. Mater.* **2008**, *18*, 1783–1789.
- 60** Nilsson, S.; Bernasik, A.; Budkowski, A.; Moons, E. *Macromolecules* **2007**, *40*, 8291–8301.
- 61** Kozub, D. R.; Vakhshouri, K.; Orme, L. M.; Wang, C.; Hexemer, A.; Gomez, E. D. *Macromolecules* **2011**, *44*, 5722–5726.
- 62** Walker, B.; Tamayo, A. B.; Dang, X.-D.; Zalar, P.; Seo, J. H.; Garcia, A.; Tantiwiwat, M.; Nguyen, T.-Q. *Adv. Funct. Mater.* **2009**, *19*, 3063–3069.
- 63** Kim, C.; Liu, J.; Lin, J.; Tamayo, A. B.; Walker, B.; Wu, G.; Nguyen, T.-Q. *Chem. Mater.* **2012**, *24*, 1699–1709.
- 64** Swartz, C. R.; Parkin, S. R.; Bullock, J. E.; Anthony, J. E.; Mayer, A. C.; G. G. Malliaras *Org. Lett.* **2005**, *7*, 3163–3166.
- 65** Li, G.; Shrotriya, V.; Huang, J.; Yao, Y.; Moriarty, T.; Emery, K.; Yang, Y. *Nat. Mater.* **2005**, *4*, 864.
- 66** Brabec, C. J. *Sol. Energy Mater. Sol. Cells* **2004**, *83*, 273.